npj Computational Materials

www.nature.com/npjcompumats

ARTICLE OPEN

Check for updates

Topological pruning enables ultra-low Rayleigh scattering in pressure-quenched silica glass

Yongjian Yang[1], Osamu Homma[2], Shingo Urata[2], Madoka Ono[3,4]✉ and John C. Mauro[1]✉

Silica glass is the most indispensable material in optical communication applications due to its superior optical properties. The transmission loss of silica glass has been reduced over the past 30 years by continuous efforts toward decreasing density fluctuations by lowering of fictive temperature, e.g., through improvements in processing or doping. A recent study has shown that shrinkage of structural voids by hot compression is a promising way to further decrease the loss. However, an atomic understanding of the pressure effect is still lacking. Here, using molecular simulations, we connect the void shrinkage to topological pruning of silica network. Two physical models predict that the Rayleigh scattering loss of pressure-quenched silica glass can be reduced by >50% when the glass is quenched at an appropriate pressure (4 GPa in our simulation). Our studies are consistent with available experimental results and demonstrate topologically optimized structure can give desirable properties for optical applications of silica as well as other glasses with similar network structure.

npj Computational Materials (2020)6:139 ; https://doi.org/10.1038/s41524-020-00408-1

INTRODUCTION

Silica (SiO_2) glass is the single most important material for fiber optic communications due to a combination of several favorable properties[1] including high optical transparency, high tensile/bending strength, good processability, ability to tune refractive index by doping, and low cost. Because of this unique combination of properties, silica glass has revolutionized global telecommunications through the development of high-bandwidth optical communication networks. During the 1970s, research was vigorously conducted to reduce the loss in silica glass by a factor of a hundred[2–4]. A 10–20% further decrease in optical attenuation has been achieved, e.g., in fluorine-doped silica glass fiber[4,5]. Interests in low optical loss are also seen in SiO_2-based waveguides that are used in planar lightwave circuits[6–8]. Notwithstanding the extreme importance of SiO_2 glass in these applications, there is a lack of atomistic level understanding of optical attenuation in the glass. In addition, the lack of recent progress in reducing optical loss is due to limitations in the processing methods that have been considered. More than 80% of the optical loss in silica glass fiber is due to Rayleigh scattering[3,9,10], which can be suppressed by reducing the density fluctuations in glass, e.g., by reducing its fictive temperature. The fictive temperature of silica can be reduced by: (a) reducing the cooling rate[1]; (b) introducing an annealing process[11]; or (c) reducing the viscosity of the glass by doping with an alkali metal oxide[12,13]. However, reductions in cooling rate or annealing cause a significant decrease in production yield, and compositional variations can lead to an increase in loss due to chemical concentration fluctuations[14]. Recent experimental reports have shown that controlling the pressure history of silica can affect the density fluctuations or heterogeneity and the Rayleigh/X-ray scattering[15,16]. This method of controlling fictive *pressure* has provide a new train of thought to achieve even lower propagation loss of silica glass. Although the silica glass structural change due to hot compression has been shown to be very different from cold-compressed silica glass with comparable density as well as the pristine silica glass[17], a systematic understanding of the pressure effect on the silica network structure in terms of homogeneity of the glass at the atomistic level is not available which is required for the design of ideal glass structure with optimal optical properties.

Hence, in this study, we use molecular dynamics (MD) simulations to examine how density fluctuation of SiO_2 glass can be suppressed under conditions of varying pressure, including conditions beyond those reported in the experiments[15]. The MD simulations provide a direct probe to the SiO_2 network structure which can be compared with experimental results for density and void size within the experimentally achievable applied pressures. The model shows that the optical loss can be improved significantly without using an extremely high pressure. We specifically show that pressure quenching leads to an enhanced homogeneity of the silica glass characterized by a decreasing void size which can be understood using topological pruning picture, bringing a significant reduction in Rayleigh scattering intensity by ~56% at a quench pressure of 4 GPa in MD. We examine details of the change in homogeneity of SiO_2 glass due to hot compression between 0 and 12 GPa and find that it is controlled by two different mechanisms depending on the magnitude of the pressure. While the homogeneity at large pressure is compromised due to an increase of network connectivity, at lower pressures, the dominant homogenization mechanism is related to the topological pruning of the network, which is found to be an effective way for tailoring of SiO_2 properties without introducing unwanted defects. These findings provide an atomistic understanding of the pressure-induced network homogenization and also shed light on topological optimization of the silica glass network for optical applications.

[1]Department of Materials Science and Engineering, The Pennsylvania State University, University Park, PA 16802, USA. [2]Innovative Technology Research Center, AGC Inc., 1150 Hazawa-cho, Kanagawa-ku Yokohama, Kanagawa 221-8755, Japan. [3]Materials Integration Laboratories, AGC Inc., 1150 Hazawa-cho, Kanagawa-ku Yokohama, Kanagawa 221-8755, Japan. [4]Research Institute for Electronic Science, Hokkaido University, Kita 20 Nishi 10, Kita-ku, Sapporo, Hokkaido 001-0020, Japan. ✉email: madoka.mo.ono@agc.com; jcm426@psu.edu

Published in partnership with the Shanghai Institute of Ceramics of the Chinese Academy of Sciences

npj nature partner journals

RESULTS

Structure of hot-compressed silica glass from MD

To demonstrate the effect of quench pressure (P_Q) on silica glass, we have conducted pressure-quench simulations of silica using the recently developed SHIK potential[18] (see "Methods" for justification of this potential and Supplementary Fig. 1a). Density obtained by experiment is well reproduced by MD simulations using SHIK potential as shown in Fig. 1 (also see Supplementary Fig. 1b). The increase of silica glass density with quench pressure is accompanied by the reduction of structural void size in the glass as illustrated in Fig. 2a. Here, isosurfaces with a minimum distance of 0.1 nm (about the size of the largest voids in α-quartz) from the surface of an atom are visualized as "voids". At $P_Q = 0$ GPa, many of the voids are interconnected in 3D space and their sizes are relatively large. From $P_Q = 0$ to 1.0 GPa, these voids become more disconnected and their sizes become significantly smaller. At $P_Q =$ 4.0 GPa, only disconnected voids remain, and the number of the voids (with a radius > 0.1 nm) are few. At $P_Q = 8.0$ GPa, the voids even disappear. Such change persists during the whole cooling procedure (see Supplementary Fig. 2). The void size distributions are shown in Fig. 2b. It shows a rapid extinction of large sized voids (radius > 0.2 nm) from ambient pressure up to 2 GPa. The largest void size in the silica glass decreases significantly with increasing P_Q as plotted in Fig. 2c. Despite the fact that the experimental data (red points) from positron annihilation lifetime spectroscopy[15] are only available up to $P_Q = 0.2$ GPa, the largest void size results from MD up to this range show a very good agreement in both the absolute value and the trend.

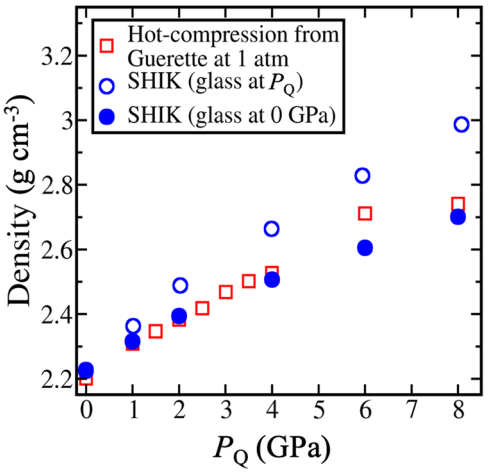

Fig. 1 Densities of the hot-compressed silica glass. The experimental data (red squares) is from Guerette et al.[17]. The compression is done at 1373 K at each corresponding pressure. The density of the MD simulated glass is on par with the pressure-quenched SiO_2 glass in experiments (the open blue circles and the filled blue circles correspond to the simulated glasses before and after the P_Q is released, respectively). For MD simulation, quenching is done from 4000 K, and same as the experiment, the quench pressure P_Q is released down to 1 atm at room temperature. The standard deviation of the density of MD glasses is around 0.007 g cm^{-3}.

The significant modification of void morphology and distribution in the pressurized silica glass suggests that some network structure change in the silica glass is triggered by the pressure quench. Here, to characterize the structural change in the SiO_2 framework, we make use of the cluster model[19,20] in which we ignore all O atoms and consider each Si atom and its Si coordination sequence $CS = \{N_k\} = N_1, N_2, \ldots, N_k$, where N_k indicates the number of Si atoms in "sphere" k which are connected to Si atoms in sphere $k-1$. A cutoff of 3.4 Å (see the "Methods") is used to find the neighbor Si atoms of each Si atom. Note that here the N_1, i.e., CN_{Si-Si} is not the same as the Si coordination, CN_{Si-O} (i.e., the coordination number of Si–O), often referred in experiments[17,21,22], which is very close to 4 in our simulations ($CN_{Si-O} \le 4.05$ at $P_Q \le 8$ GPa, see Supplementary Fig. 4) and consistent with other simulations[23]. It has also been shown[23,24] that a slower cooling rate such as the 1 K ps^{-1} used in current study tends to generate a $CN_{Si-O} = 4$ network when the SiO_2 glass density is less than 2.7 g cm^{-3} (or $P_Q < 8$ GPa). An example of CS is shown in the inset of Fig. 3b (left panel) wherein

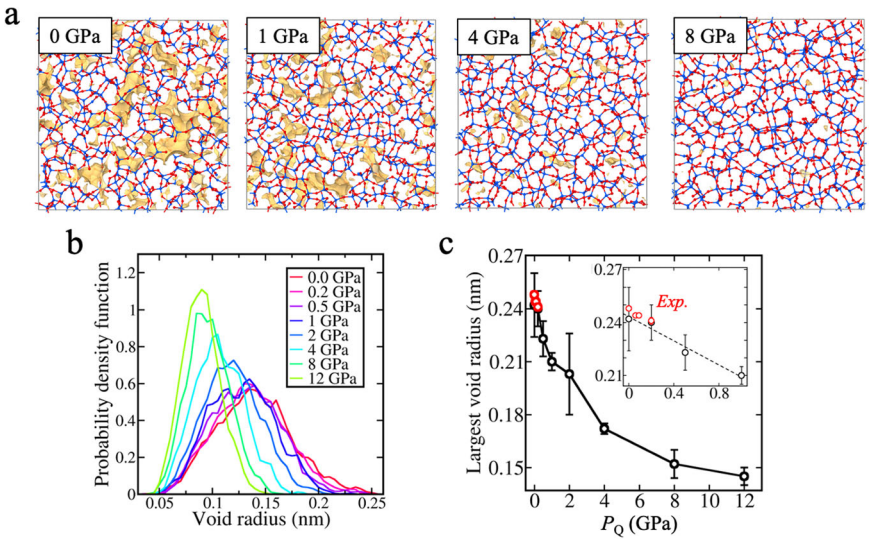

Fig. 2 Pressure effects on voids in silica glass. a Morphologies of voids in four silica glass samples pressure-quenched at 0, 1, 4, and 8 GPa (P_Q has been released). The yellow regions are isosurfaces with a minimum distance of 0.1 nm from the surface of any atoms in the glass. In other words, voids with a radius <0.1 nm are not shown. The blue and red atoms are Si and O, respectively. Only a slice of the glass (~10 Å thick) is visualized for clearness. **b** Void radius distributions at different pressures. The curves are smoothed using a moving average with a step of 0.05 nm. **c** Variation of the largest void radius from both experiments (red, up to 0.2 GPa) and MD simulations. The inset is a close-up view of the pressure region from 0 to 1 GPa where the dashed line is a guide for eyes to show the consistent trends between the simulation results and the positron annihilation lifetime spectroscopy experiments[15]. The error bar is calculated from the standard deviation of multiple samples.

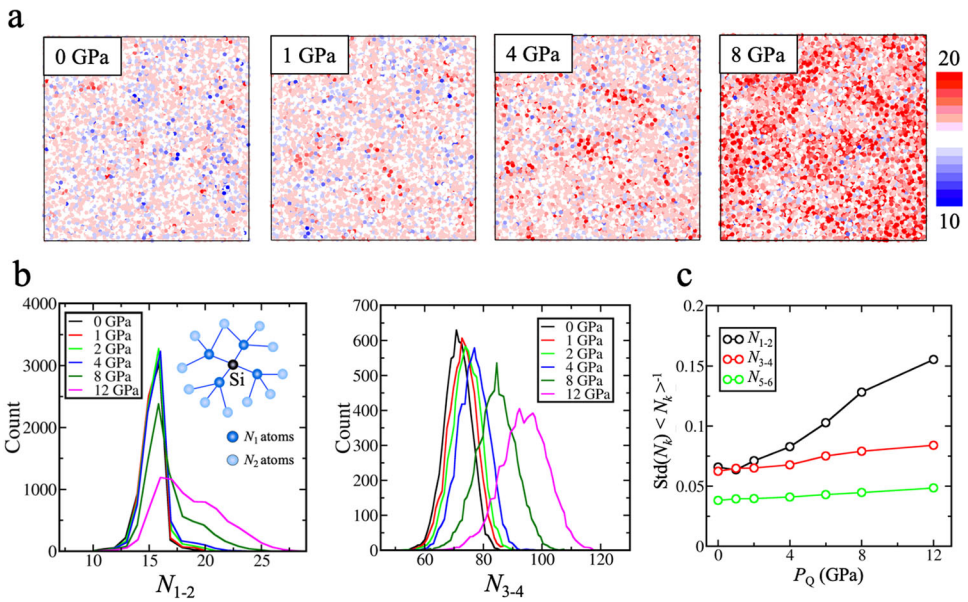

Fig. 3 Local Si neighbor number in silica glass. a Spatial distribution of N_{1-2} ($=N_1 + N_2$) of each Si atom in the silica glass samples pressure quenched at $P_Q = 0$, 1, 4, and 8 GPa. The color scheme is shown on the right hand. **b** Statistical distribution of N_{1-2} and N_{3-4} in the pressure-quenched silica glass. The inset in **b** gives an example in which the central Si atom (black) has four first neighbor Si atoms (blue, $N_1 = 4$) and eleven second neighbor Si atoms (light blue $N_2 = 11$). **c** Variation of normalized standard deviation (Std) of N_k as a function of the quench pressure.

the central Si atom has $N_1 = 4$ and $N_2 = 11$. The spatial distribution of N_{1-2} (i.e., $N_1 + N_2$) in the silica glass and its statistics are shown in Fig. 3a, b from which a significant increase in the dispersion of N_{1-2} appears when P_Q increases from 4 to 8 GPa. Likewise, the dispersion of the N_{3-4} (Fig. 3b, right panel) is also seen to increase more significantly at $P_Q > 4$ GPa. The normalized standard deviation (Std (N_k) $<N_k>^{-1}$) in N_k is shown in Fig. 3c, where a larger increase of variation in the Si coordination sequence is seen in N_{1-2} (the 1st and 2nd neighboring Si atoms) than in N_{3-4} and so forth in N_{5-6}. The change in the 1st (locating at ~3 Å away) and the 2nd (locating at ~5 Å away) neighboring Si atoms is consistent with the major variation in void size as shown in Fig. 2 particularly in those voids whose diameter is between 2 and 4 Å (note the atomic radius of Si (0.26 Å) and O (1.35 Å) are taken into account). The large variation in N_k in Fig. 3b, especially in N_{1-2} also suggests that the homogeneity of the silica glass would deteriorate when P_Q is too high and different CN_{Si-Si} appears.

Calculation of Rayleigh scattering of densified silica glass

As a result of decreasing void size, Rayleigh scattering is expected to be significantly reduced with improvement of the glass homogeneity. The Rayleigh scattering can be quantified via either Mie theory or density fluctuations (see "Methods"). The Rayleigh scattering intensity R_{sp} of all voids can be calculated using the following equation based on the Mie theory[25] which sums contribution from all N voids in the material by treating them as scattering spherical particles,

$$R_{sp} = \frac{1}{V}\sum_{i=1}^{N}\frac{2}{3}\pi^5\left(\frac{n^2-1}{n^2+2}\right)^2\frac{D_i^6}{\lambda^4}, \quad (1)$$

where V is the volume of the material, n is the relative refractive index, D_i is the diameter of the ith void and λ is the wavelength the incoming light. R_{sp} calculated from all voids (see "Methods" and Fig. 2b) is plotted against P_Q in Fig. 4a by the blue curve. The plot shows a clear suppression of R_{sp} (e.g., ~57% from 0 to 4 GPa or ~65% when 8 GPa ≤ P_Q ≤ 12 GPa). While it is difficult to directly obtain the Rayleigh scattering coefficient α_{scat} from R_{sp}, we have attempted to convert R_{sp} to α_{scat} at 1.55 μm via two SiO_2 samples from MD whose largest pore sizes are similar as two SiO_2 samples from experiments[15] whose α_{scat} values are known (see "Methods"). Such obtained α_{scat} value for each MD SiO_2 sample is shown using the right axis of Fig. 4a. The inset of Fig. 4a compares the MD results with the available experimental α_{scat} available up to $P_Q =$ 0.2 GPa[15] where a suppression in α_{scat} is seen in both cases. The amount of change in α_{scat} from MD seems to be smaller than the experiments at 0.2 GPa, which may result from several factors: (1) the inaccuracy of the conversion from R_{sp} to α_{scat} (only the largest pore is considered), (2) the simple treatment of pore as spherical particles in the Mie theory while their shapes are irregular as shown in Fig. 2a, and/or (3) the much shorter time scale used in MD under high pressure than experiments.

Alternatively, we may calculate α_{scat} from the density fluctuations of the silica glass. As noted in "Methods", α_{scat} can be written in terms of density fluctuations $\frac{\langle N^2\rangle - \langle N^2\rangle}{\langle N\rangle}$ as[10,26]:

$$\alpha_{scat} = (10\log_{10} e)\frac{8\pi^3}{3\lambda^4}n^8p^2\frac{\langle N^2\rangle - \langle N^2\rangle}{\langle N\rangle\overline{n}}, \quad (2)$$

where λ is the wavelength, n is refractive index, p is the photoelastic coefficient, and $\overline{n}$ is the number density of particles. N is the number of particles in volume V and the angle brackets indicate an average. The density fluctuation $\frac{\langle N^2\rangle - \langle N\rangle^2}{\langle N^2\rangle}$ can be calculated from density/volume variation of multiple samples melt-quenched using, e.g., the NPT ensemble. Given the empirical relation between n and ρ (the density of a glass in g cm^{-3})[17,27], i.e., $n = (\rho - 2.21) \times 0.193 + 1.46$, the photoelastic constant p for an isotropic solid can be calculated as $\frac{2\rho}{n^3}\frac{\partial n}{\partial \rho}$[10,28] which, when substituted in Eq. 2, would reduce the dependence on n from the eighth power to the second power. Use of this empirical relation is justified because the relative error of n is <2% based on ref. [27] which would at most cause a relative error of ~4% in α_{scat}. α_{scat} as a function of quench pressure using Eq. (2) is shown in Fig. 4b. The Rayleigh scattering is found to be suppressed at $P_Q =$ 4 GPa with a reduction of 56% compared with at 0 GPa which is very close to the reduction in R_{sp} (57%) from Fig. 4a. Specifically, a scattering loss ~0.081 dB km^{-1} due to Rayleigh scattering can be achieved at 4 GPa, which is in the same ballpark as the Rayleigh

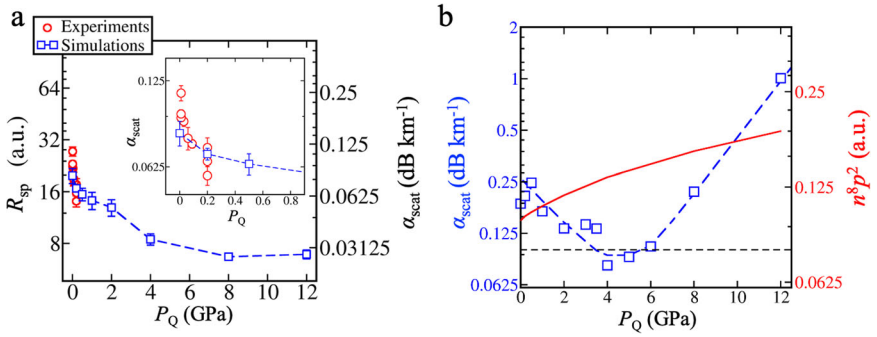

Fig. 4 Rayleigh scattering of pressure-quenched SiO_2 glasses at a wavelength of 1.55 μm. a Calculated R_{sp} (left axis) at different P_Q using the Mie theory and the corresponding α_{scat} at $\lambda = 1.55$ μm (right axis). Experimental results from ref. [15] are also included for comparison. Note that the experimental data in Fig. 3a contain SiO_2 glasses quenched using the same pressure but different holding times or different glass transition temperature; therefore, multiple values exist at $P_Q = 0.0$ and 0.2 GPa. The error bars are estimated by the difference between the largest R_{sp} and the smallest R_{sp} at each P_Q. **b** Calculated α_{scat} and n^8p^2 at different quench pressures using density fluctuations. Each α_{scat} is calculated from density variation of eighteen samples (see "Methods"). Additional data from SiO_2 samples with different P_Q are added to obtain the trend for α_{scat}. The blue dashed line is an eye guide to show the trend of α_{scat}. The black dashed line corresponds to 0.1 dB km^{-1}.

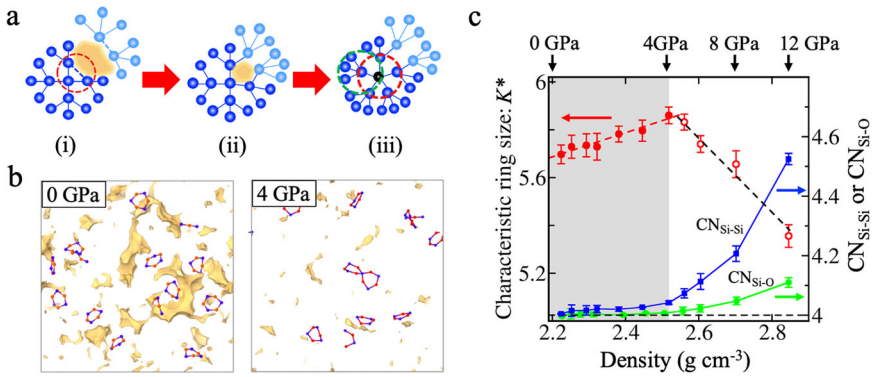

Fig. 5 Homogenization mechanism of silica glass. a Configurational change to account for the homogenization effect (via elimination of a three-membered ring[29,30] as denoted in the red circle) and dehomogenization effect (via introduction of different CN_{Si-Si}) at high P_Q in the SiO_2 glass. The yellow area denotes a void whose size decreases after the exemplary three-membered ring is eliminated. All spheres denote the Si atoms (the O atoms are not considered). **b** Proximity of free space to 3-memberd rings (Si: blue atoms and O: red atoms) in silica glasses whose $P_Q = 0$ and 4 GPa. The yellow regions are isosurfaces with a minimum distance of 0.11 nm from the surface of any atoms in the glass. **c** Characteristic ring size K^* (red) and CN_{Si-Si} or CN_{Si-O} at different densities. CN_{Si-Si} is defined as the average number of first Si neighbor atoms to a central one using a cutoff of 3.4 Å. The dashed red line and black dashed line are guides for eyes. Multiple samples were used to calculate the standard deviation for the error bar.

scattering loss of conventional/hot-compressed silica in experiments[11,15] and is extremely low given the much higher cooling rate used in MD (1 K ps^{-1}). However, a further increase of P_Q to 12 GPa will instead enhance the scattering by more than 10 times, in contrast with Fig. 4a, suggesting that factors other than voids should be considered at higher pressure. Figure 4b also shows the change of the n^8p^2 term in Eq. (2) with a monotonic increasing trend with P_Q (e.g., an increase of 37% is seen from 0 to 4 GPa), confirming that the lowering of α_{scat} comes solely from change of glass homogeneity. We note here that even though it seems that predictions using Mie theory gives smaller α_{scat} than those from density fluctuation, both Fig. 4a, b show that a reduction of Rayleigh scattering by ~56% can be achieved using a moderate quench pressure ~4 GPa. The calculated value of α_{scat} using void-scattering and density fluctuation models are, respectively, 0.069 and 0.21 dB km^{-1} under 0.2 GPa. Although the former value matches well with the experimental results (~0.06–0.07 dB km^{-1}) as shown by the inset of Fig. 4a, we believe the latter value is more accurate when considering the high cooling rate and the short P_Q holding time used in the MD simulations. The fictive temperatures (>2100 K) of the SiO_2 glasses in MD simulations are several hundred degrees higher than the experimental samples, suggesting that an extremely low Rayleigh scattering coefficient may be achieved by tailoring the thermal history of the glass in combination with its pressure history as reported by ref. [15]. The results of α_{scat} calculation using void-scattering and density fluctuation both clearly indicate that, by increasing P_Q from 0.0 to 4 GPa, a continuous decrease of α_{scat} is expected. Such improvement in α_{scat} should come from amelioration of homogeneity of silica glass as evidenced in Fig. 2.

Understanding the homogenization of silica glass

To understand the homogenization mechanism of the silica network as a result of P_Q, we examine the structural differences among those glasses. We evaluate the change of ring size distribution (whose calculation method is described in "Methods" and see Supplementary Fig. 3) for the simulated silica glass. For P_Q < 6 GPa, CN_{Si-O} in the silica glass remains close to 4.0 and the Si–Si distance scarcely changes (see Fig. 5c, Supplementary Fig. 4 and Supplementary Methods). The improvement in SiO_2 homogeneity can be understood using the topological pruning mechanism (Fig. 5a)[29,30] which, to our knowledge, has only been used to account for the densification of SiO_2 network. According to refs. [29,30], ring formation reduces the density of the network by *pruning* a calculable number of tetrahedrally coordinated atoms

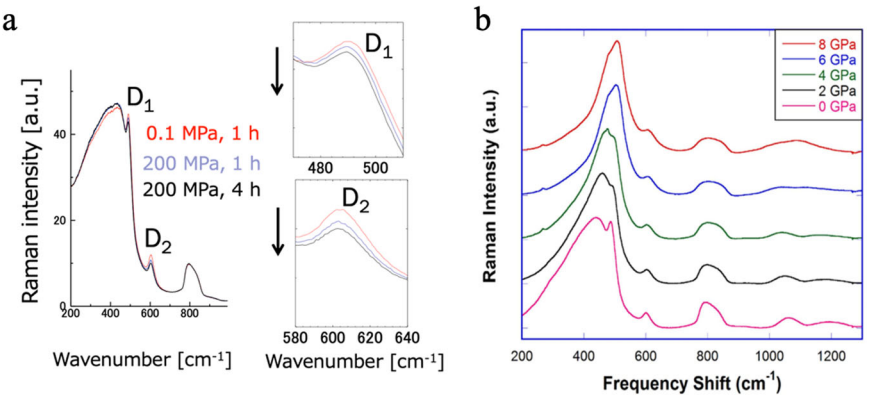

Fig. 6 Raman spectrum of silica glass. a Raman spectrum of three pressure-quenched silica glass samples prepared at 0.1 MPa for 1 h, 0.2 GPa for 1 h, and 0.2 GPa for 4 h, all at 2073 K. The variations of the relative intensity of the D_1 and D_2 peaks as a function of time are enlarged for clarity on the right. **b** Raman spectrum of pressure-quenched SiO_2 glasses from higher pressures at 1373 K by Guerette et al.[17].

(Si atoms) and the relative ability of different sized rings to reduce the network density decreases exponentially with the ring size K. Therefore, a higher density of SiO_2 can be achieved by eliminating smaller rings as illustrated in Fig. 5a: (i)–(ii) and increasing the characteristic ring size K^* (see Supplementary Methods for calculation of K^*). At $P_Q \le 4$ GPa, small ring ratios ($K \le 7$) are found mostly to decrease with P_Q (see Supplementary Fig. 3B, D) and K^* approaches 6 as shown in Fig. 5a. Note a linear increase of K^* in the simulated glass with pressure at $P_Q \le 4$ GPa is observed, which means that the glass network should become more homogeneous in the sense that its K^* is closer to that of the quartz (whose K^* is between 6 and 8) whose a_{scat} is extremely small (<0.01 dB km^{-1} using $k_B T\beta_T$[31] where $T = 300$ K and $\beta_T = 2.68 \times 10^{-11}$ Pa[32]). In order to further correlate such change to the void result (Fig. 2), we propose an alternative way to account for the homogeneity improvement via the proximity of free space, i.e., voids, to smaller rings ($K \le 7$) which, partially, can be pruned to densify the glass. An example is given in Fig. 5a: (i)–(ii) in which the free space (yellow region) near the 3-member ring shrinks after the ring is pruned to allow additional Si atoms (light blue) to connect with the group of dark blue Si atom. Similar mechanism can also occur at the proximity of 4 and 5 membered rings. The proximity of the free space to 3-membered rings is evidenced in Fig. 5b (also for $K = 4$ in Supplementary Fig. 5) at 0 GPa. Unlike the shrinkage of pores due to distortion of the rings under pressure which tends to recover once P_Q is released, this achievement in homogenization requires breaking and forming of bonds which shall persist after P_Q is released at the room temperature.

On the other hand, large rings ($K > 7$) increase, and particularly, small rings ($K < 6$) are found to significantly rebound at $P_Q > 4$ GPa (see Supplementary Fig. 3b). This change in the constituent ratio of the ring size comes from the increase of CN_{Si-Si} in the silica glass as shown in Fig. 5a: (ii)–(iii), leading to an increase in density fluctuation as shown by the different number of Si atoms enclosed by the red and green circles in Fig. 5a (iii) and the local Si neighbor number shown in Fig. 3. We note that the increase in the constituent ratio of small rings is also seen before P_Q is released (Supplementary Fig. 3c), which is consistent with experimental results under high pressure by Hemley et al.[33] and ab initio calculations by Trave et al.[34] and Karki et al.[35] of the silica liquid.

Although there is no consensus on the change of the populations of the 3- and 4-membered rings with pressure in silica glass/liquid from previous MD simulation results[17,29,34–36] probably due to the usage of different simulation settings, e.g., the interatomic potential, the cooling rate, the pressure condition, the ring concepts, etc., our ring statistics seem to be supported experimentally by the change of the two defect peaks, D_1 and D_2, arising from symmetric stretch of regular 4-membered rings and 3-membered rings[37,38]. Figure 6a shows our Raman measurements from the samples used in ref. [15]. Both D_1 and D_2 peaks are found to decrease in intensity without any frequency shift at higher pressure and at longer holding time, when the silica glasses are quenched from 2073 K with one at ambient pressure and two others held at 200 MPa for 1 and 4 h prior to the quench, suggesting a smaller population of the two types of the rings due to hot compression. The weakening (between 0 and 4 GPa) of the two peaks is also observed by the Raman spectrum results of SiO_2 glass by Guerette et al.[17] (Fig. 6b) quenched from a lower temperature 1373 K. Instead, at large pressures, e.g., 8 GPa, the intensities of the two peaks seem to be enhanced according to Fig. 6b using the right-most point as the reference. By comparison, the intensity of the D_2 peak of silica glass subjected to cold compression increases monotonically with the maximal pressure reached[39]. Here, we have several remarks. First, although experiments show that the CN_{Si-O} of hot-compressed silica remains at close to 4 with P_Q up to 8 GPa[17,21], they do not preclude CN_{Si-Si} from being higher than 4 as shown in Fig. 5c. Second, due to the much higher cooling rate used in MD, it is likely that the increase of CN_{Si-O} and CN_{Si-Si} may be postpone at some P_Q value larger than 4 GPa if a slow cooling rate is used. However, heterogeneity shall occur as long as a coexistence of different CN_{Si-O}/CN_{Si-Si} starts to appear which will enhance optical scattering[16]. Lastly, based on the works by Bridgman[40–42], Vukcevich[43] has shown a maximal compressibility is reached for cold-compressed silica glass under a pressure between 3 and 4 GPa. However, this is different from the observed lowest density fluctuation of the hot-compressed silica glass in our simulations which corresponds to a minimal compressibility at around 4 GPa (see Supplementary Fig. 1d).

DISCUSSION

The change of density fluctuations in SiO_2 glass with P_Q can now be clearly understood in terms of the two topological modification of SiO_2 network. At $P_Q < 4$ GPa, decrease of population of smaller rings and increase of larger ring population drive the network to be closer to a perfect Bethe lattice (Fig. 5a) whose density fluctuations is extremely low (all lattice points have equal chemical sequence). Such tendency of SiO_2 structure to approach the Bethe lattice can lead to a decrease in void size (Fig. 5a). At higher P_Q, the equality of the Bethe lattice points is undermined by appearance of Si atoms with different CN_{Si-Si}, leading to an increased density fluctuation. Thus, the highest homogeneity of silica glass is achieved at some intermediate value of P_Q (~4 GPa) in our MD simulations. Lastly, the high cooling rate used in MD may shift the critical pressure to a smaller value above which

CN_{Si-O} and CN_{Si-Si} start to increase rapidly. This suggests that further improvement in Rayleigh loss can be achieved by using a slower cooling rate at a higher P_Q.

Previous MD results by Kaiki et al.[35] show that the Grüneisen parameter and heat capacity of the liquid SiO_2 have distinct values in this low-pressure regime ($P \le 4$ GPa). While a complete analysis of these properties is beyond the scope of this study, the SiO_2 structure between 0 and 4 GPa changes solely in the ring structure without introduction of defects, e.g., under- or over-coordinated Si/O atoms, with adverse effect on optical properties. Our study, therefore, shows a topological way of improving the optical properties of silica glass which may be applicable in other network glasses such as GeO_2 and B_2O_3. Lastly, while it is tempting to connect the characteristic ring size K^* to the void size in SiO_2, according to our results (Figs. 2b, 5b), they vary with P_Q in opposite directions at $P_Q < 4$ GPa, which suggests that the ring pruning should play a critical role in the homogenization.

To sum up, we have shown that, using the pressure-quench method and two different methods to calculate Rayleigh loss, the homogeneity of silica glass can be significantly improved, achieving a reduction in Rayleigh scattering by more than 50%. Given the different simulation conditions compared to experiments, the improvement in loss is expected to be even greater if lower cooling rates are used. Such improvement is due to the homogenization in the pressurized silica network. Specifically, at $P_Q \le 4$ GPa, the reduction in density fluctuation results from a change in intermediate-range order that is supported by Raman spectrum and ring structure analysis in our MD simulations and can be understood as an approaching of the network's characteristic ring size to a perfect Bethe lattice. Higher values of P_Q, however, are found to potentially bring about coexistence of different network coordinations which will undermine the homogeneity of the network. Our findings have shown, through an atomistic understanding, how the homogeneity of SiO_2 is improved by pressure; topological pruning from decrease of small rings can drive the network to be more like a Bethe lattice and at the same time decrease those voids close to the pruned rings without introducing unwanted defects. This provides not only the detailed understanding of the structural change induced by hot compression, but also an example of ideal SiO_2 glass structure of high homogeneity which is desirable for optical applications. Such ideal glass structure is useful not only for silica glass, but also for other types of inorganic glass with similar network structure such as GeO_2. Although a high P_Q at high temperature is still technically challenging, the ideal glass structure might be approachable using other techniques such as high-pressure chemical vapor deposition[44,45], which might be applied to improve the optical transparency of light waveguide.

METHODS

Molecular dynamics simulations

Silica glass samples were generated by randomly distributing 3000 atoms in a cubic box and melted in the liquid state at 4000 K at different pressures for 100 ps, followed by a quenching process to 300 K at a rate of 1 K ps^{-1}. It has also been shown[23,24] that a slower cooling rate such as the 1 K ps^{-1} used in current study tends to generate a $CN_{Si-O} = 4$ SiO_2 network when the SiO_2 glass density is less than 2.7 g cm^{-3} ($P_Q < 8$ GPa according to Fig. 1). The quench pressure $P_Q = 0$–12 GPa is maintained using a Nosé–Hoover thermostat/barostat[46–48] in the isothermal–isobaric ensemble (NPT). Larger samples of 24,000 atoms were used to get the cooling curves (e.g., Fig. 1) and measure the density fluctuation. After the melt-quench, the pressure is reduced to 1 atm in 100 ps followed by an additional run for 100 ps at 1 atm. The SHIK potential[18] used for the atomic interaction has been found to accurately reproduce radial distribution function (RDF) of silica liquid[18], vibrational density of states[18], and the density of glass at 300 K at various pressures. The Si speciation in liquid SiO_2 predicted by this potential also compares well with ab initio calculation and TS potential considering O polarizability (see Supplementary Fig. 1c). For comparison, BKS potential[49,50] broadly applied for SiO_2 simulations is also used to generate silica glass by pressure quench of the liquid from 7000 to 300 K using the same cooling rate (see Supplementary Fig. 1b). Note a higher cooling rate is used in ref. [24], making the resulted glass densities different from us. All MD simulations and structure visualizations are carried out using LAMMPS[51] and OVITO[52], respectively.

Structural analysis

A cutoff of 2.2 Å is used for Si–O pair, and 3.4 Å for Si–Si pair for bond angle and coordination analysis. These values are the position of the first minimum in the corresponding RDFs. The void and its distribution was obtained using Zeo++[53,54]. Shannon radii[55] for Si, 0.26 Å and O, 1.35 Å are used to define the surface of an atom and for the void analysis, which are very close to the radii determined in ref. [22]. The void radius distribution from Zeo++ does not give the number of voids. To calculate the total amount of voids, we use the surface area function in Zeo++ to obtain the number of voids whose radii are larger than a critical value so that they comprise of the largest ~20% voids using Fig. 2b. The total number of voids is then calculated by dividing this number with this percent. The R.I.N.G.S. code[56] was used to determine the primitive ring distribution.

Raman spectroscopy

Raman spectra were collected with a Raman microscope (Nicolet Almega, Thermo Fisher Scientific Inc., Yokohama, Japan) in backscattering geometry. The excitation wavelength was 532 nm. Polished plates with dimensions of 15 × 15 × 1 mm were used for the measurements. 100× microscope and 1800 l mm^{-1} grating were used. Data were taken with the exposure time set as 60 s, with accumulation of 10 times. All measurements were conducted at room temperature (around 300 K).

Calculation of Rayleigh scattering (R_{sp} and α_{scat})

The R_{sp} can be directly calculated using Eq. (1) and the total number of voids and the void distribution obtained from Zeo++[53,54]. Two methods were used to calculate the Rayleigh attenuation α_{scat}. In method I (see Eq. (3)), the following equation is assumed to derive α_{scat} from R_{sp} for the MD simulated silica glasses,

$$\alpha_{scat} = A \log_{10}\left[1 - B R_{sp}\right] = C \cdot R_{sp}, \quad (3)$$

where A, B, and C are constants and the second equation is valid when the term inside the logarithmic function is close to 1. Two SiO_2 samples pressure-quenched at 0 and 0.2 GPa in the current MD simulation whose largest pore sizes (0.2435 and 0.2415 nm) and densities (2.210 and 2.215 g cm^{-3}) are similar to two of the experimental samples in ref. [15] (0.2436 nm and 0.2414 nm, and 2.230 g cm^{-3} and 2.256 g cm^{-3}) whose α_{scat} are known. C are found to be 4.14×10^{-3} dB km^{-1} μm^{-4}. In method II, we directly calculate the density fluctuation (both configurational and vibrational ones are included) which causes the Rayleigh scattering of pure SiO_2 glass. The density fluctuation is described by[57,58],

$$\left(\frac{\langle N^2\rangle - \langle N^2\rangle}{\langle N\rangle \bar{n}}\right)_{\mu VT} = \left(\frac{\langle V^2\rangle - \langle V^2\rangle}{\langle V\rangle}\right)_{NPT} = k_B T \beta_T, \quad (4)$$

where N is the number of particles in volume V, $\bar{n}$ is the number density, k_B is the Boltzmann's constant, T is the temperature, β_T is the isothermal compressibility, and angle brackets indicate an average. μVT and NPT represent the grand canonical ensemble and the isothermal–isobaric ensemble, respectively. Because all MD simulations were carried out using the NPT ensemble, we have used volume variation of multiple glass samples instead of variation of the number of particles to calculate the density fluctuation. Data reported are from 18 samples prepared under similar conditions but different initial configurations.

DATA AVAILABILITY

Details of the simulations are available within the article. All data supporting the findings of this study are available from the authors upon reasonable request.

Received: 25 May 2020; Accepted: 26 August 2020;
Published online: 17 September 2020

REFERENCES

1. Varshneya, A. K. & Mauro, J. C. *Fundamentals of Inorganic Glasses*, Ch. 1 (Elsevier, 2019).
2. Nishimura, Y. '*Electronic Industry History' 1981: Optical Fiber Communication*, 156202 (Nikkei Electronics, 2008).
3. Miya, T., Terunuma, Y., Hosaka, T. & Miyashita, T. Ultimate low-loss single-mode fiber at 1.55 µm. *Electron. Lett.* **15**, 106–108 (1979).
4. Tamura, Y. et al. The first 0.14-dB/km loss optical fiber and its impact on submarine transmission. *J. Light. Technol.* **36**, 44–49 (2018).
5. Tamura, Y. et al. Lowest-ever 0.1419-dB/km loss optical fiber. *In Optical Fiber Communication Conference and Exhibition*, 1–3 (2017).
6. Lee, H., Chen, T., Li, J., Painter, O. & Vahala, K. J. Ultra-low-loss optical delay line on a silicon chip. *Nat. Commun.* **3**, 1–7 (2012).
7. Takada, K., Yamada, H., Hida, Y., Ohmori, Y. & Mitachi, S. Rayleigh backscattering measurement of 10 m long silica-based waveguides. *Electron. Lett.* **32**, 1665–1667 (1996).
8. Miya, T. Silica-based planar lightwave circuits: passive and thermally active devices. *IEEE J. Sel. Top. Quantum Electron.* **6**, 38–45 (2000).
9. Tsujikawa, K., Tajima, K. & Ohashi, M. Rayleigh scattering reduction method for silica-based optical fiber. *J. Light. Technol.* **18**, 1528–1532 (2000).
10. Olshansky, R. Propagation in glass optical waveguides. *Rev. Mod. Phys.* **51**, 341–367 (1979).
11. Saito, K. et al. Limit of the Rayleigh scattering loss in silica fiber. *Appl. Phys. Lett.* **83**, 5175–5177 (2003).
12. Saito, K., Ikushima, A. J., Ito, T. & Itoh, A. A new method of developing ultralow-loss glasses. *J. Appl. Phys.* **81**, 7129–7134 (1997).
13. Anderson, J., Ellison, A. & Schiefelbein, S. Method of doping silica glass with an alkali metal, and optical fiber precursor formed therefrom. *U.S. Patent Application US2006/0130530 A1* (2006).
14. Kakiuchida, H., Saito, K. & Ikushima, A. J. Rayleigh scattering in fluorine-doped silica glass. *Jpn. J. Appl. Phys.* **42**, 6516–6517 (2003).
15. Ono, M., Aoyama, S., Fujinami, M. & Ito, S. Significant suppression of Rayleigh scattering loss in silica glass formed by the compression of its melted phase. *Opt. Express* **26**, 7942–7948 (2018).
16. Sato, T., Funamori, N., Wakabayashi, D., Nishida, K. & Kikegawa, T. Coexistence of two states in optically homogeneous silica glass during the transformation in short-range order. *Phys. Rev. B* **98**, 144111 (2018).
17. Guerette, M. et al. Structure and properties of silica glass densified in cold compression and hot compression. *Sci. Rep.* **5**, 1–10 (2015).
18. Sundararaman, S., Huang, L., Ispas, S. & Kob, W. New optimization scheme to obtain interaction potentials for oxide glasses. *J. Chem. Phys.* **148**, 194504 (2018).
19. Meier, W. & Moeck, H. The topology of three-dimensional 4-connected nets: classification of zeolite framework types using coordination sequences. *J. Solid State Chem.* **27**, 349–355 (1979).
20. Brunner, G. O. The properties of coordination sequences and conclusions regarding the lowest possible density of zeolites. *J. Solid State Chem.* **29**, 41–45 (1979).
21. Xue, X., Stebbins, J. F., Kanzaki, M., McMillan, P. F. & Poe, B. Pressure-induced silicon coordination and tetrahedral structural changes in alkali oxide-silica melts up to 12 GPa: NMR, Raman, and infrared spectroscopy. *Am. Mineral.* **76**, 8–26 (1991).
22. Zeidler, A., Salmon, P. S. & Skinner, L. B. Packing and the structural transformations in liquid and amorphous oxides from ambient to extreme conditions. *Proc. Natl Acad. Sci. U.S.A.* **111**, 10045–10048 (2014).
23. Koziatek, P., Barrat, J. L. & Rodney, D. Short- and medium-range orders in as-quenched and deformed SiO_2 glasses: an atomistic study. *J. Non-Cryst. Solids* **414**, 7–15 (2015).
24. Yuan, F. & Huang, L. Brittle to ductile transition in densified silica glass. *Sci. Rep.* **4**, 5035 (2014).
25. Bohren, C. F. & Huffman, D. R. *Absorption and Scattering of Light by Small Particles*, Ch. 5 (John Wiley & Sons, 2008).
26. Pinnow, D. A., Rich, T. C., Ostermayer, F. W. & DiDomenico, M. Fundamental optical attenuation limits in the liquid and glassy state with application to fiber optical waveguide materials. *Appl. Phys. Lett.* **22**, 527–529 (1973).
27. Tan, C. Z., Arndt, J. & Xie, H. S. Optical properties of densified silica glasses. *Phys. B Condens. Matter* **252**, 28–33 (1998).
28. Schroeder, J., Mohr, R., Macedo, P. B. & Montrose, C. J. Rayleigh and Brillouin scattering in K_2O-SiO_2 Glasses. *J. Am. Ceram. Soc.* **56**, 510–514 (1973).
29. Stixrude, L. & Bukowinski, M. S. T. A novel topological compression mechanism in a covalent liquid. *Science* **250**, 541–543 (1990).
30. Stixrude, L. & Bukowinski, M. Rings, topology, and the density of tectosilicates. *Am. Mineral.* **75**, 1159–1169 (1990).
31. Saito, K., Kakiuchida, H. & Ikushima, A. J. Investigation of the origin of the Rayleigh scattering in SiO_2 glass. *J. Non-Cryst. Solids* **222**, 329–334 (1997).
32. Brace, W. F., Schulz, C. H. & La Mori, P. N. Isothermal compressibility of kyanite, andalusite, and sillimanite from synthetic aggregates. *J. Geophys. Res.* **74**, 2089–2098 (1969).
33. Hemley, R. J., Mao, H. K., Bell, P. M. & Mysen, B. O. Raman spectroscopy of SiO_2 glass at high pressure. *Phys. Rev. Lett.* **57**, 747–750 (1986).
34. Trave, A., Tangney, P., Scandolo, S., Pasquarello, A. & Car, R. Pressure-induced structural changes in liquid SiO_2 from ab initio simulations. *Phys. Rev. Lett.* **89**, 245504 (2002).
35. Karki, B. B., Bhattarai, D. & Stixrude, L. First-principles simulations of liquid silica: Structural and dynamical behavior at high pressure. *Phys. Rev. B* **76**, 104205 (2007).
36. Kubicki, J. D. & Lasaga, A. C. Molecular dynamics simulations of SiO_2 melt and glass: Ionic and covalent models. *Am. Mineral.* **73**, 941–955 (1988).
37. Galeener, F. L. Band limits and the vibrational spectra of tetrahedral glasses. *Phys. Rev. B* **19**, 4292–4297 (1979).
38. Geissberger, A. E. & Galeener, F. L. Raman studies of vitreous SiO_2 versus fictive temperature. *Phys. Rev. B* **28**, 3266–3271 (1983).
39. Deschamps, T. et al. Permanent densification of compressed silica glass: a Raman-density calibration curve. *J. Phys. Condens. Matter* **25**, 025402 (2013).
40. Bridgman, P. W. The compression of 39 substances to 100,000 kg/cm^2. *Proc. Am. Acad. Arts Sci.* **76**, 55–70 (1948).
41. Bridgman, P. The compression of sixty-one solid substances to 25,000 kg/cm^2, determined by a new rapid method. *Proc. Am. Acad. Arts Sci.* **76**, 9–24 (1945).
42. Bridgman, P. W. Certain physical properties of single crystals of tungsten, antimony, bismuth, tellurium, cadmium, zinc, and tin. *Proc. Am. Acad. Arts Sci.* **60**, 305–383 (1925).
43. Vukcevich, M. R. A new interpretation of the anomalous properties of vitreous silica. *J. Non-Cryst. Solids* **11**, 25–63 (1972).
44. Araki, S., Mohri, N., Yoshimitsu, Y. & Miyake, Y. Synthesis, characterization and gas permeation properties of a silica membrane prepared by high-pressure chemical vapor deposition. *J. Membr. Sci.* **290**, 138–145 (2007).
45. Singh, S., Ediger, M. D. & de Pablo, J. J. Ultrastable glasses from in silico vapour deposition. *Nat. Mater.* **12**, 139–144 (2013).
46. Nosé, S. A unified formulation of the constant temperature molecular dynamics methods. *J. Chem. Phys.* **81**, 511–519 (1984).
47. Hoover, W. G. Canonical dynamics: equilibrium phase-space distributions. *Phys. Rev. A* **31**, 1695–1697 (1985).
48. Hoover, W. G. Constant-pressure equations of motion. *Phys. Rev. A* **34**, 2499–2500 (1986).
49. Carré, A., Berthier, L., Horbach, J., Ispas, S. & Kob, W. Amorphous silica modeled with truncated and screened Coulomb interactions: a molecular dynamics simulation study. *J. Chem. Phys.* **127**, 114512 (2007).
50. Van Beest, B., Kramer, G. J. & Van Santen, R. Force fields for silicas and aluminophosphates based on ab initio calculations. *Phys. Rev. Lett.* **64**, 1955–1958 (1990).
51. Plimpton, S. Fast parallel algorithms for short-range molecular dynamics. *J. Comput. Phys.* **117**, 1–19 (1995).
52. Stukowski, A. Visualization and analysis of atomistic simulation data with OVITO–the open visualization tool. *Model. Simul. Mater. Sci. Eng.* **18**, 015012 (2010).
53. Willems, T. F., Rycroft, C. H., Kazi, M., Meza, J. C. & Haranczyk, M. Algorithms and tools for high-throughput geometry-based analysis of crystalline porous materials. *Microporous Mesoporous Mater.* **149**, 134–141 (2012).
54. Pinheiro, M. et al. Characterization and comparison of pore landscapes in crystalline porous materials. *J. Mol. Gr. Model.* **44**, 208–219 (2013).
55. Shannon, R. D. & Prewitt, C. T. Effective ionic radii in oxides and fluorides. *Acta Crystallogr. B* **25**, 925–946 (1969).
56. Le Roux, S. & Jund, P. Ring statistics analysis of topological networks: new approach and application to amorphous GeS_2 and SiO_2 systems. *Comput. Mater. Sci.* **49**, 70–83 (2010).
57. Watanabe, T., Saito, K. & Ikushima, A. J. Fictive temperature dependence of density fluctuation in SiO_2 glass. *J. Appl. Phys.* **94**, 4824–4827 (2003).
58. Allen, M. P. & Tildesley, D. J. *Computer Simulation of Liquids,* Ch. 2 (Oxford University Press, 2017).

ACKNOWLEDGEMENTS

Y.Y. and J.C.M. acknowledge financial support from AGC Inc. and the Institute for CyberScience Advanced CyberInfrastructure (ICS-ACI) at The Pennsylvania State University. Y.Y. acknowledges Siddharth Sundararaman for SHIK potential file and technical support from Christopher Blanton at ICS-ACI. We also thank Kazutaka Hayashi, Akio Koike, and Yuki Kondo from AGC Inc. for fruitful discussions.

AUTHOR CONTRIBUTIONS

M.O. and J.C.M. designed the project. Y.Y. performed the molecular simulations, which Y.Y., M.O., S.U., and J.C.M. analyzed. O.H. performed the Raman spectroscopy experiments and analyzed the data. All authors participated in discussing the data. Y.Y., M.O., and J.C.M. wrote the paper with input from all authors.

COMPETING INTERESTS

The authors declare no competing interests.

ADDITIONAL INFORMATION

Supplementary information is available for this paper at https://doi.org/10.1038/s41524-020-00408-1.

Correspondence and requests for materials should be addressed to M.O. or J.C.M.

Reprints and permission information is available at http://www.nature.com/reprints

Publisher's note Springer Nature remains neutral with regard to jurisdictional claims in published maps and institutional affiliations.